Density Functional Study on Acid Stability of Mn, Ni, and Fe Dual Atom Catalyst Active Sites Embedded in Graphene

Muhammad Lukmanul Hakim[1,2], Adhitya Gandaryus Saputro[1,3,4]* & Ganes Shukri[1,3,4]

[1] Graduate Program of Engineering Physics, Faculty of Industrial Technology, Institut Teknologi Bandung, Bandung, West Java 40132, Indonesia
[2] PT PLN (Persero), Indonesia
[3] Quantum and Nano Technology Research Group, Faculty of Industrial Technology, Institut Teknologi Bandung, 40132 Bandung, Indonesia
[4] Research Centre for Nanoscience and Nanotechnology, Institut Teknologi Bandung, Bandung, West Java 40132, Indonesia
*Email: gandaryus@itb.ac.id
Email: Email Address

Abstract. This study investigates the stability of Mn, Ni, and Fe dual atom catalyst (DAC) embedded in the basal plane of 2D graphene using density functional theory (DFT) calculations. Our results indicate that these DACs exhibit optimal performance only under specific alkaline conditions. Pourbaix diagrams were constructed to assess the stability of both configurations, revealing that Mn DACs offer a broader operational range in the unpoisoned state compared to Fe and Ni DACs. For the ortho configuration, the active sites are predicted to remain unpoisoned, avoiding adsorption by intermediates such as O* and OH*. However, the para configuration of all three DACs remains functional only in their poisoned states. These findings provide valuable insights for the design of DAC-based ORR catalysts, suggesting that ortho configurations should be studied under conditions where the active sites remain bare, while para configurations should be investigated under poisoned states.

Keywords: *Acid Stability, DAC, ORR, DFT, Active site poisoning*.

1 Introduction

The Proton Exchange Membrane Fuel Cell (PEMFC) is a clean and efficient energy conversion device used to convert hydrogen into electrical energy, particularly in electric vehicle applications. The device operates through hydrogen oxidation to protons at the anode and oxygen reduction at the cathode, with water being the only byproduct [1]. Currently, platinum (Pt) is the catalyst of choice for the oxygen reduction reaction (ORR) due to its high activity and excellent stability [2]. However, Pt's high cost and scarcity necessitate the search for alternative catalysts. Several studies have explored non-precious metal

Received _____, Revised _____, Accepted for publication _____

catalysts that can replace Pt, emphasizing ORR activity, stability, and cost-effectiveness [3–5]. Among these alternatives, transition metal-nitrogen-carbon (M-N-C, where M can be Fe, Co, Mn, Ni, etc.) catalysts have demonstrated the most promising performance [6–12]. Despite these advances, the stability of some non-precious metal catalysts remains a challenge in acidic environments, and further improvements are required.

Recent studies have shown that increasing the metal dopant content in 2D materials can effectively enhance the catalytic activity and stability of single-atom catalysts (SACs) [13–15]. Additionally, diatomic-transition metal doped graphene catalysts have shown superior ORR activity compared to their single-atom counterparts [14–19]. Previous work by Karmodak and colleagues[15], reported that dual atom catalysts (DACs) based on Mn, Fe, and Ni integrated into the graphene framework exhibit excellent ORR activity and stability over a wide pH and potential range. However, detailed information on the active site configurations in this working range is still lacking. This information is crucial, as certain DAC configurations, such as *para* active site, are only stable when the active site is poisoned by intermediates like O* and OH*, while the bare active sites tend to be unstable in a normal electrochemical condition.

This study focuses on the investigation of acid stability and demetallation behavior of Ni, Fe, and Mn DACs active sites ($M_1M_2N_6C$) under hydrogen fuel cell operating conditions using density functional theory (DFT)-based calculations. By evaluating various demetallation scenarios, we construct Pourbaix diagrams for these catalysts to identify their stable working conditions, particularly in the presence of potential active site poisoning.

2 Methods

Spin-polarized DFT, as implemented in the Quantum ESPRESSO package, was used to perform the geometric optimization and calculate the system's total energy [20]. Ultrasoft pseudopotentials were used to describe the electron-ion interactions [21], and a plane-wave basis set was employed with a kinetic energy cutoff of 50 Ry and an electron density cutoff of 600 Ry [22–25]. The Generalized Gradient Approximation (GGA) within the Perdew-Burke-Ernzerhof (PBE) functional handled the exchange-correlation effects [26]. For the 2D graphene sheets, we applied a 2 x 2 x 1 Monkhorst-Pack k-point grid [27]. A vacuum layer of 15 Å was added along the normal direction to the graphene surface to prevent spurious interactions between periodic images. Finally, the atomic structures were relaxed until the Hellmann-Feynman forces acting on each atom were reduced to less than 0.05 eV/Å.

We constructed Pourbaix diagrams to analyze the stability of $NiNiN_6C$, $FeFeN_6C$, and $MnMnN_6C$ active sites over a range of pH values and applied potentials. This allowed us to identify the conditions that maximize the catalyst stability during the ORR process. The ion demetallation mechanism was investigated for two typical DAC configurations: *ortho* $[(M_1M_2N_6)_o]$ and *para* $[(M_1M_2N_6)_p]$, as depicted in **Figure 1** [28,29].

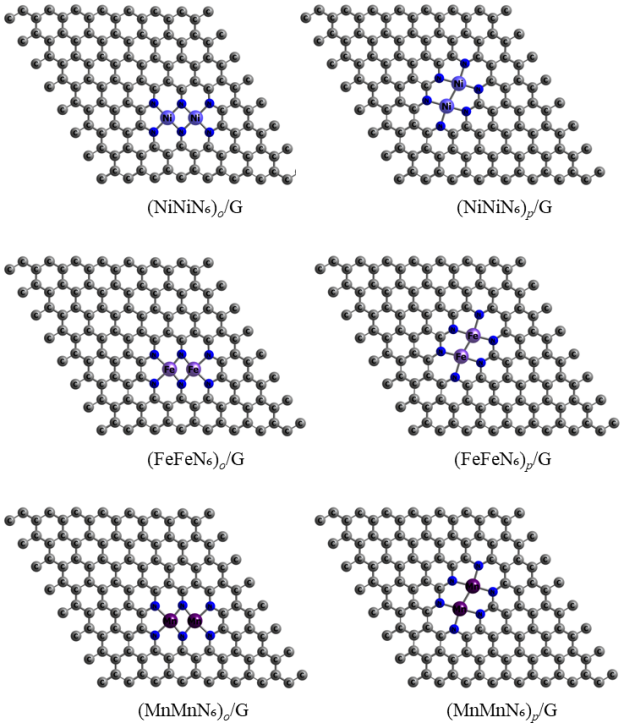

Figure 1 Two typical DAC configurations: *ortho* $[(M_1M_2N_6)_o]$ and *para* $[(M_1M_2N_6)_p]$.

During demetallation, transition metal ions are released from the $MnMnN_6C$, $NiNiN_6C$, and $FeFeN_6C$ structures, transitioning into aqueous ions and leaving behind cavities within the graphitic structure, which vary in their degree of protonation [30]. This demetallation process affects both clean active sites and those with adsorbed ORR intermediates. Prior studies have shown that adsorbed OH* and O* species can thermodynamically stabilize single-atom catalysts (SACs) across a broad pH range. Consequently, we also need to consider the role of these intermediates in stabilizing Mn, Ni, and Fe DACs active sites during demetallation. The demetallation process for DAC Mn, Ni, and Fe is hypothesized to follow one of the pathways described below [15,30,31].

$$M_1M_2N_6C/O_aH_b + nH^+ \leftrightarrow M^P_{1/2} + \frac{b}{2}O_2 + M_{2/1}N_6CH_{n+a} + (p-n)e^- \quad (1)$$

$$M_1M_2N_6C/O_aH_b + nH^+ \leftrightarrow M^P_1 + M^q_2 + \frac{b}{2}O_2 + N_6CH_{n+a} + (p+q-n)e^- \quad (2)$$

$$M_1M_2N_6C/O_aH_b + (2a-b+n)H^+_n \leftrightarrow M^P_{1/2} + aH_2O + M_{2/1}N_6CH + (p-(2a-b+n))e^- \quad (3)$$

$$M_1M_2N_6C/O_aH_b + (2a-b+n)H^+ \leftrightarrow M^P_1 + M^q_2 + aH_2O + N_6CH_m + ((p+q)-(2a-b+n))e^- \quad (4)$$

The structure $M_1M_2N_6C$ corresponds to the bare active site (**Figure 1**), whereas the configuration $M_1M_2N_6C/O_aH_b$, represents the active site with adsorbed O* (a=1, b=0) or OH* (a=1, b=1) intermediates. The variables *p* and *q* represent the oxidation states of the dissolved ions, while *n* denotes the number of protons involved in the demetallation reaction. In this study, we examined *n*-values ranging from 0 to 6.

The equilibrium potentials under specific pH conditions for reactions (1)–(4) were calculated using the Nernst equation [32]:

$$U_{red} = U^{(0)}_{red} - \frac{RT}{nF} ln \frac{[\text{Product}]}{[\text{Reactant}]} \quad (5)$$

Based on previous studies [30,33], this equation can be grouped into two distinct cases. The pH-dependent equilibrium potential U_{eq}(pH), which establishes equilibrium lines for reactions where $p+q \neq n$, is determined by solving the following equation:

$$U_{eq}(pH)_{p+q\neq n} = \frac{(\Delta G)_{pH=0}}{(p+q-n)} + \frac{n}{(p+q-n)} pH\, k_B T \ln 10 \quad (6)$$

For cases where $p+q = n$, representing a proton-balanced state, the equilibrium pH is plotted as a vertical line, calculated using the following general expression:

$$pH_{eq;p+q=n} = \frac{\Delta G_{pH=0}}{-nk_B T\, ln\, 10} \quad (7)$$

The free energy difference between products and reactants, $\Delta G = G_{products} - G_{reactants}$, defines the thermodynamic favorability of a reaction, determining its direction and extent. A negative ΔG indicates that the reaction is spontaneous under the specified conditions.

The free energy associated with the dissolved transition metal ion is calculated as follows[31]:

$$G(M^{x+}) = E_{DFT(bulk)} + \Delta G_x \quad (8)$$

Here, ΔG_x refers to the free reaction energy of the bulk metal demetalation process, derived from literature [32,34,35]. For these calculations, the dissolved metal ion concentration is assumed to be 1 M at a temperature of 298.15 K.

3 Results

3.1 Ni DAC Active Sites

In the NiNi DAC system, the $(NiNiN_6)_o$/G and $(NiNiN_6)_p$/G configurations are only stable under alkaline conditions, with a relatively narrow working range of pH and potential as shown in **Figure 2**. In the *ortho* case, O* and OH* phases do not appear, mainly because NiNi sites generally exhibit weaker adsorption ability compared with MnMn and FeFe. As a result, the O* and OH* phases are not sufficiently facilitated. This behaviour is also observed in certain Ni-SAC configurations [31]. However, in the *para* configuration, the O* and OH* phases can be stabilised, with working conditions similar to the $(NiNiN_6)_p$/G configuration. This is due to the stronger adsorption ability of the *para* configuration compared to the *ortho* configuration [28,29]

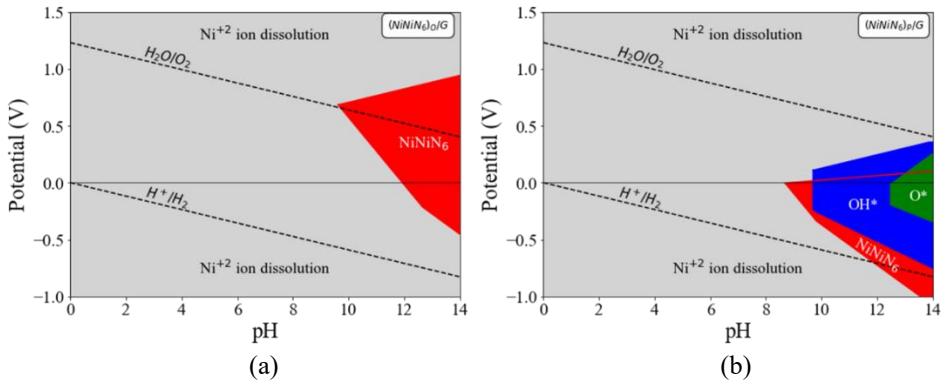

Figure 2 Pourbaix diagram of (a) $(NiNiN_6)_o$/G, (b) $(NiNiN_6)_p$/G.

3.2 Fe DAC Active Sites

The results of the study for the $FeFeN_6C$ active site as per **Figure 3** differ from those reported by Karmodak [15] where its working range is reported to cover all pH levels, including both acidic and alkaline conditions. Consistent with some experiments on Fe DAC and Fe SAC, our calculations show that these catalysts can only operate optimally under alkaline conditions [36,37]. Unlike Ni DAC with *ortho* configuration case, the O* and OH* phases can be stabilised at a similar working range with $(FeFeN_6)_o$/G in the *clean* phase. However, from

previous research [28], $(FeFeN_6)_o$/G shows good ORR activity at relatively high potential, which facilitates the reduction of O* and OH* to H_2O easily. Consequently, in practice, the *clean* $(FeFeN_6)_o$/G active site (red region in **Figure 3a**) will dominate the active site configuration under its working condition.

In contrast, the working range of the *para* $(FeFeN_6)_p$/G active site in the *clean* phase is very narrow as shown in **Figure 3b**, because even at low potential, the active site is poisoned by O* and OH* due to the strong binding energy of molecules in the *para* configuration [28]. As a result, the active site of $(FeFeN_6)_p$/G is effectively a poisoned site, to which O* and OH* have been bound.

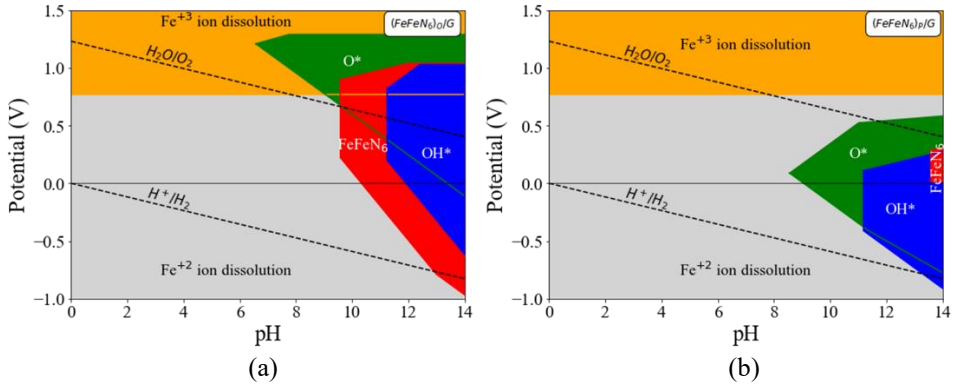

Figure 3 Pourbaix diagram of (a) $(FeFeN_6)_o$/G, (b) $(FeFeN_6)_p$/G.

3.3 Mn DAC Active Sites

Similar to the case of $FeFeN_6$, and contrary to the findings of [15], however our analysis of the adsorbate revealed that the *ortho* and *para* configurations of $MnMnN_6$ are unstable under acidic conditions as shown in **Figure 4**. Interestingly, the active site of $(MnMnN_6)_o$/G *clean* phase exhibits a wider working range than $(FeFeN_6)_o$/G, with stability at pH > 5, while the O* and OH* poisoned states occur in a potential range of > 5 with stability at pH > 5, while the O* and OH* poisoned states occur in the same potential range. Previous research suggests this site has a good ORR rate, is unlikely to be O* and OH* poisoned, and the active site configuration for the *ortho* configuration will be dominated by the plain $(MnMnN_6)_o$/G state in its working state [15].

For the *para* configuration, our findings show that the *clean* $(MnMnN_6)_p$/G operates in a very narrow working range under alkaline conditions, which indicates that this *clean* structure is not effective as an ORR catalyst. This is in line with previous studies [15]. However, when the site is poisoned by O* and

OH*, its working range widens significantly. Generally, *para-type* catalysts are always poisoned by O* or OH*, and thus, in practice, poisoned *para* catalysts are expected to function over a larger pH range. Therefore, further research is needed to investigate the ORR activity of $(MnMnN_6)_p$/G under poisoned conditions.

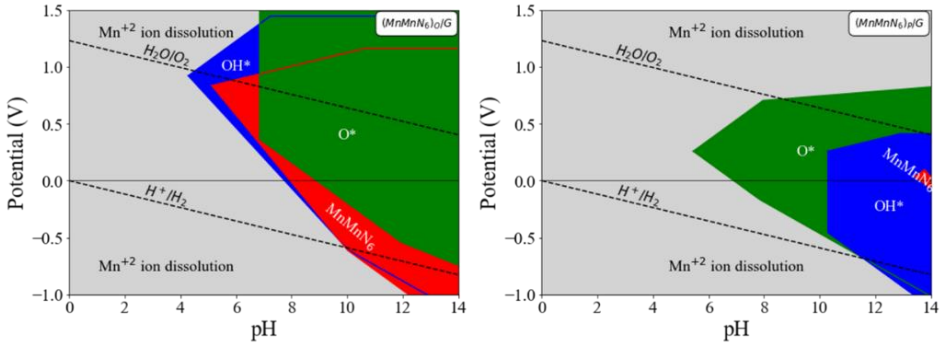

Figure 4 Pourbaix diagram of (a) $(MnMnN_6)_o$/G, (b) $(MnMnN_6)_p$/G

4 Conclusion

We have studied the stability of Mn, Fe, and Ni DACs active sites using DFT-based calculations. We discovered that these DAC active sites are only functional under certain alkaline conditions. In all cases of the *ortho* configuration, the active sites are predicted to remain in the bare state without being poisoned. Meanwhile, for the *para* configuration, the strong binding affinity for adsorbates results in the active sites being consistently poisoned by O* and OH*. Therefore, to study the ORR activity of the *ortho* configuration, it is recommended to focus on the bare active site, whereas for ORR in the *para* configuration, it is advised to consider the active site in the poisoned state with O* and OH*.

Acknowledgement

We acknowledge the research funding provided by Institut Teknologi Bandung under the 'Riset Unggulan ITB' grant scheme. Some of the calculations were conducted using the HPC facility at the Research Center for Nanosciences and Nanotechnology (RCNN), Institut Teknologi Bandung. We also extend our gratitude to the Distance Learning Program in collaboration with PLN and ITB, which supported the successful completion of this work.

References

[1] Zhang, G., Chenitz, R., Lefèvre, M., Sun, S., & Dodelet, J.-P., "Is iron involved in the lack of stability of Fe/N/C electrocatalysts used to reduce oxygen at the cathode of PEM fuel cells," Nano Energy, 29, pp. 111-125, Feb. 2016. (Journal)

[2] Nørskov, J.K., Rossmeisl, J., Logadottir, A., Lindqvist, L., Kitchin, J.R., Bligaard, T., et al., "Origin of the Overpotential for Oxygen Reduction at a Fuel-Cell Cathode," J. Phys. Chem. B, 108, pp. 17886-17892, 2004. (Journal)

[3] Xia, W., Mahmood, A., Liang, Z., Zou, R., & Guo, S., "Earth-Abundant Nanomaterials for Oxygen Reduction," Angewandte Chemie International Edition, 55, pp. 2650-2676, 2016. (Journal)

[4] Thompson, S.T., & Papageorgopoulos, D., "Platinum group metal-free catalysts boost cost competitiveness of fuel cell vehicles," Nat. Catal., 2, pp. 558-561, 2019. (Journal)

[5] He, Y., Liu, S., Priest, C., Shi, Q., & Wu, G., "Atomically dispersed metal–nitrogen–carbon catalysts for fuel cells: advances in catalyst design, electrode performance, and durability improvement," Chem. Soc. Rev., 49, pp. 3484-3524, 2020. (Journal)

[6] Lefèvre, M., Proietti, E., Jaouen, F., & Dodelet, J.-P., "Iron-Based Catalysts with Improved Oxygen Reduction Activity in Polymer Electrolyte Fuel Cells," Science (1979), 324, pp. 71-74, 2009. (Journal)

[7] Proietti, E., Jaouen, F., Lefèvre, M., Larouche, N., Tian, J., Herranz, J., et al., "Iron-based cathode catalyst with enhanced power density in polymer electrolyte membrane fuel cells," Nat. Commun., 2, pp. 416, 2011. (Journal)

[8] Shui, J., Chen, C., Grabstanowicz, L., Zhao, D., & Liu, D.-J., "Highly efficient nonprecious metal catalyst prepared with metal–organic framework in a continuous carbon nanofibrous network," Proceedings of the National Academy of Sciences, 112, pp. 10629-10634, 2015. (Journal)

[9] Liu, Q., Liu, X., Zheng, L., & Shui, J., "The Solid-Phase Synthesis of an Fe-N-C Electrocatalyst for High-Power Proton-Exchange Membrane Fuel Cells," Angewandte Chemie International Edition, 57, pp. 1204-1208, 2018. (Journal)

[10] Chung, H.T., Cullen, D.A., Higgins, D., Sneed, B.T., Holby, E.F., More, K.L., et al., "Direct atomic-level insight into the active sites of a high-performance PGM-free ORR catalyst," Science, 357, pp. 479-484, 2017. (Journal)

[11] Wang, L., Wan, X., Liu, S., Xu, L., & Shui, J., "Fe-N-C catalysts for PEMFC: Progress towards the commercial application under DOE reference," J. Energy Chem., 39, pp. 77-87, 2019. (Journal)

[12] Wan, X., Liu, X., Li, Y., Yu, R., Zheng, L., Yan, W., et al., "Fe–N–C electrocatalyst with dense active sites and efficient mass transport for high-performance proton exchange membrane fuel cells," Nat. Catal., 2, pp. 259-268, 2019. (Journal)
[13] Chen, Z., Higgins, D., Yu, A., Zhang, L., & Zhang, J., "A review on non-precious metal electrocatalysts for PEM fuel cells," Energy Environ Sci, 4, pp. 3167-3192, 2011. (Journal)
[14] Pedersen, A., Barrio, J., Li, A., Jervis, R., Brett, D.J.L., Titirici, M.M., et al., "Dual-Metal Atom Electrocatalysts: Theory, Synthesis, Characterization, and Applications," Adv Energy Mater, 12, pp. 2102715, 2022. (Journal)
[15] Karmodak, N., & Nørskov, J.K., "Activity and Stability of Single- And Di-Atom Catalysts for the O2 Reduction Reaction," Angewandte Chemie International Edition, 62, e202311113, 2023. (Journal)
[16] Wang, J., Huang, Z., Liu, W., Chang, C., Tang, H., Li, Z., et al., "Design of N-Coordinated Dual-Metal Sites: A Stable and Active Pt-Free Catalyst for Acidic Oxygen Reduction Reaction," J. Am. Chem. Soc., 139, pp. 17281-17284, 2017. (Journal)
[17] Yang, G., Zhu, J., Yuan, P., Hu, Y., Qu, G., Lu, B.-A., et al., "Regulating Fe-spin state by atomically dispersed Mn-N in Fe-N-C catalysts with high oxygen reduction activity," Nat. Commun., 12, pp. 1734, 2021. (Journal)
[18] Han, X., Ling, X., Yu, D., Xie, D., Li, L., Peng, S., et al., "Atomically Dispersed Binary Co-Ni Sites in Nitrogen-Doped Hollow Carbon Nanocubes for Reversible Oxygen Reduction and Evolution," Advanced Materials, 31, pp. 1905622, 2019. (Journal)
[19] Li, F., Ding, X.-B., Cao, Q.-C., Qin, Y.-H., & Wang, C., "A ZIF-derived hierarchically porous Fe–Zn–N–C catalyst synthesized via a two-stage pyrolysis for the highly efficient oxygen reduction reaction in both acidic and alkaline media," Chem. Commun., 55, pp. 13979-13982, 2019. (Journal)
[20] Giannozzi, P., Baroni, S., Bonini, N., Calandra, M., Car, R., Cavazzoni, C., et al., "QUANTUM ESPRESSO: a modular and open-source software project for quantum simulations of materials," J. Phys.: Condens. Matter, 21, pp. 395502, 2009. (Journal)
[21] Rappe, A.M., Rabe, K.M., Kaxiras, E., & Joannopoulos, J.D., "Optimized pseudopotentials," Phys. Rev. B, 41, pp. 1227-1230, 1990. (Journal)
[22] Dipojono, H.K., Saputro, A.G., Fajrial, A.K., Agusta, M.K., Akbar, F.T., Rusydi, F., et al., "Oxygen reduction reaction mechanism on a phosphorus-doped pyrolyzed graphitic Fe/N/C catalyst," New J. Chem., 43, pp. 11408-11418, 2019. (Journal)
[23] Fajrial, A.K., Abdulkarim, M., Saputro, A., Agusta, M.K., Tapran, N., & Dipojono, H., "Boron and Nitrogen Co-doping Configuration on Pyrolyzed

Fe-N4/C Catalyst," Procedia Eng., 170, pp. 131-135, 2017. (Conference Proceedings)
[24] Saputro, A.G., Fajrial, A.K., Agusta, M.K., & Dipojono, H.K., "Density Functional Study on the Formation of Sulfur-doped Configuration on the Active Site of Pyrolyzed Fe/N/C Catalyst," J. Phys. Conf. Ser., 1204, pp. 012119, 2019. (Conference Proceedings)
[25] Saputro, A.G., Fajrial, A.K., Maulana, A.L., Fathurrahman, F., Agusta, M.K., Akbar, F.T., et al., "Dissociative Oxygen Reduction Reaction Mechanism on the Neighboring Active Sites of a Boron-Doped Pyrolyzed Fe–N–C Catalyst," J. Phys. Chem. C, 124, pp. 11383-11391, 2020. (Journal)
[26] Perdew, J.P., Burke, K., & Ernzerhof, M., "Generalized Gradient Approximation Made Simple," Phys. Rev. Lett., 77, pp. 3865-3868, 1996. (Journal)
[27] Monkhorst, H.J., & Pack, J.D., "Special points for Brillouin-zone integrations," Phys. Rev. B, 13, pp. 5188-5192, 1976. (Journal)
[28] Sumbowo, J.F., Ihsan, F.A., Fathurrahman, F., Amalia, N., Akbar, F.T., Yudistira, H.T., et al., "Graphene-edge-supported iron dual-atom for oxygen reduction electrocatalysts," Phys. Chem. Chem. Phys., 25, pp. 32637-32647, 2023. (Journal)
[29] Nuruddin, A., Saputro, A.G., Maulana, A.L., Rusydi, F., Akbar, F.T., Yudistira, H.T., et al., "Selectivity of CO2 reduction reaction to CO on the graphitic edge active sites of Fe-single-atom and dual-atom catalysts: A combined DFT and microkinetic modeling," Carbon Resour. Convers., 7, pp. 100185, 2024. (Journal)
[30] Holby, E.F., Wang, G., & Zelenay, P., "Acid Stability and Demetalation of PGM-Free ORR Electrocatalyst Structures from Density Functional Theory: A Model for 'Single-Atom Catalyst' Dissolution," ACS Catal., 10, pp. 14527-14539, 2020. (Journal)
[31] Patniboon, T., & Hansen, H., "Acid-Stable and Active M–N–C Catalysts for the Oxygen Reduction Reaction: The Role of Local Structure," ACS Catal., 11, pp. 13102-13118, 2021. (Journal)
[32] Pourbaix, M., *Atlas of Electrochemical Equilibria in Aqueous Solutions*, 2nd ed., National Association of Corrosion Engineers, Houston, Tex., 1974. (Book)
[33] Persson, K.A., Waldwick, B., Lazic, P., & Ceder, G., "Prediction of solid-aqueous equilibria: Scheme to combine first-principles calculations of solids with experimental aqueous states," Phys. Rev. B, 85, pp. 235438, 2012. (Journal)
[34] Haynes, W.M., *CRC Handbook of Chemistry and Physics*, CRC Press, 2016. (Book)

[35] Bratsch, S.G., "Standard Electrode Potentials and Temperature Coefficients in Water at 298.15 K," J. Phys. Chem. Ref. Data, 18, pp. 1-21, 1989. (Journal)
[36] Zhang, W., Yi, S., Yu, Y., Liu, H., Kucernak, A., Wu, J., et al., "Fe-based dual-atom catalysts for the oxygen reduction reaction," J. Mater. Chem. A Mater., 12, pp. 87-112, 2024. (Journal)
[37] Wang, Y., Li, S., Xu, R., Chen, J., Hao, Y., Li, K., et al., "Dual Metal Site Fe Single Atom Catalyst with Improved Stability in Acidic Conditions," Catalysts, 13, pp. 418, 2023. (Journal)